Optimizing Harmonic Mitigation for Smooth Integration of Renewable Energy: a Novel Approach Using Atomic Orbital Search and Feedback Artificial Tree Control

B. Kiruthiga, R. Karthick, I. Manju, and Krishnaveni Kondreddi

***Abstract*—This paper proposes an intelligent hybrid method for reducing harmonics to enhance power quality in a distribution system based on renewable energy sources. The proposed intelligent method, namely, the AOS-FAT technique, consolidates atomic orbital search (AOS) and a feedback artificial tree (FAT). The main objective of the proposed approach is to improve the quality of power by mitigating the harmonics. The AOS method is used to find the best values for basic and harmonic loop settings, like the shunt active power filter's direct current, voltage and the voltage at the terminals. Based on the change in load and PV parameters, a dataset variation is generated based on the objective function for minimum error. The optimal control signals are then generated using the FAT approach, which predicts the optimal parameters from the accomplished datasets. The proposed approach mitigates the overall harmonic distortion through the switching control pulses to enhance power quality. The control method concentrates on improving the maximum PV power when there is harmonic distortion by inserting the exact compensation current via the hybrid shunt active power filter. The proposed approach is implemented in MATLAB, and its performance is examined by comparing to existing methods. From the simulation outcome, the maximum PV power is 12 kW, and the THD is 1.1%.**

***Index Terms*—Shunt active power filters (SAPF), nonlinear load, maximum PV power, power quality (PQ), harmonics.**

Received: September 20, 2023
Accepted: December 15, 2023
Published Online: July 1, 2024

B. Kiruthiga (corresponding author) is with the Department of Electrical and Electronics Engineering, Velammal College of Engineering and Technology, Madurai 625009, India (kirthiice@gmail.com).

R. Karthick is with the Department of Computer Science and Engineering, K.L.N. College of Engineering, Sivagangai, India (karthickkiwi@gmail.com).

I. Manju is with the Department of Electronics and Communication Engineering, Mohamed Sathak A J College of Engineering, Chennai, India (manjujackin@gmail.com).

Krishnaveni Kondreddi (krishnaveni_eee@cbit.ac.in).

DOI: 10.23919/PCMP.2023.000577

I. Introduction

Harmonic mitigation is important for renewable energy systems connected to distribution systems [1]. Some of the more important power quality (PQ) issues in the distribution systems include power blackout, flicker, harmonics, notching transients, sags, and swells [2], [3]. System voltage variation is primarily caused by over-loading [4], [5], while non-sinusoidal current is caused by non-linear loads that produce harmonics in the voltage and current [6], [7]. These harmonics can cause detrimental effects on gear types of distribution systems (DSs), malfunction of defensive devices, overheating of transformers and rotating machines, capacitor bank damage, non-linear loading of sandwiched bus bars, etc. [8]–[10]. Many techniques have been introduced to mitigate such issues caused by harmonics [11], [12], e.g., a harmonic filtration system is used in industrial power systems to minimize harmonic distortion [13].

Examples of the harmonics produced in the load include those in static volt-ampere reactive compensators, switch-mode power supplies, inverters, DC converters, lightning strikes, AC or DC motor drives, and capacitor switching, and electric arc furnaces [14]. These disruptions lead to malfunction, reduced lifespan, and blocking of electrical components [15]. Various approaches have been used for harmonic reduction, e.g., differential evolution algorithms, recursive least squares, etc. [16]. The error value is analyzed by recursive least squares among the filter output and preferred signal in [17], though the recursive least squares has some drawbacks, such as its multifaceted and unstable nature[18]. Various evaluations are used for continuous functional improvement but they involve a large processing time [19]. To mitigate harmonics there are various choices, e.g., line reactors, harmonic traps, rectifiers, and low pass filters as presented in [20]–[23].

The harmonic mitigation component ensures the suppression of harmonics without causing negative effect on the electrical system [24]–[26]. However,

some other components' performance is based on the system condition [27]. Hence, to solve these problems, advanced approaches are needed for reducing the harmonics. The APF is frequently used to lower system harmonics [28]. This generates certain electrical components using power electronics technologies to discard the harmonic current produced by non-linear loads [29]. The compensation voltage or current reference estimator obtains the information on harmonic current and the variables of different systems. These are then used to operate the whole system controller [30]. Finally, a gating signal generator, controlled by the estimator, generates the gate signals to control power circuits [31]. The primary benefit of APF over a passive filter is the mitigation of current harmonics, while also suppressing the reactive current [32], [33]. The main contributions and novelty of this paper can be summarized as:

1) This research addresses the issue of power quality degradation in renewable energy integrated distribution systems, primarily caused by harmonics.

2) The paper introduces a hybrid approach aimed at improving the power quality in distribution systems that rely on renewable energy sources. This strategy's main goal is to mitigate harmonics.

3) The AOS method is employed to optimize datasets related to basic and harmonic loop parameters, including parameters such as the direct current voltage of the shunt APF (SAPF) and terminal voltage. These datasets are optimized based on linear and non-linear load variations, and photovoltaic (PV) parameters, with the goal of minimizing error.

4) The FAT approach is used to generate optimal control signals. This involves predicting the optimal parameters from the optimized datasets obtained through the AOS method.

5) The generated control signals are then used to eliminate overall harmonic distortion through switching control pulses.

6) A specific focus is given on improving the maximum power output from PV sources while addressing harmonic distortion. This is achieved by injecting a precise compensation current using a hybrid SAPF.

7) The proposed approach is implemented and tested using Matlab. Comparisons with existing approaches, such as enhanced particle swarm optimization (EPSO), fuzzy logic control (FLC), and sliding mode control (SMC), reveal significant improvements.

8) The simulation results demonstrate the effectiveness of the method, achieving a maximum PV power output of 12 kW while keeping the THD at a low level of 1.1%. These results indicate a significant improvement in power quality and renewable energy utilization.

The remainder of the manuscript paper is arranged as follows. Section II reviews recent research work, while Section III explains the structure of an SAPF connected PV system. Section IV explains the control structure of the half-bridge interleaved buck SAPF (HBIB-SAPF). Section V describes the proposed approach for harmonic reduction. Section VI gives the results and discussion, and Section VII concludes the paper.

II. A Brief Review of Recent Research

There has been a lot of studies on the mitigation of harmonic resonance in distribution systems using various methods and aspects. Some of them are reviewed here.

Reference [34] addresses the PQ problem for the standalone MG system by using SAPF. The continuous input current flow, constant DC-link capacitor voltage, and low switching loss are the main requirements of SAPF. As the conventional voltage source inverters (VSI) do not provide these, a split source inverter (SSI) is introduced. Using the same mechanism of VSI and modulation index, the SSI controls both the AC and DC sides. In [35], a damping approach is suggested for minimizing the loss of SAPF with an LCL filter. The suggested approach is dependent on the auxiliary converter and is incorporated with the filter capacitor, whereas the voltage of the system is controlled by an auxiliary converter. In order to lower the system's harmonics, Reference [36] proposes an adaptive neuro-fuzzy inference system that makes use of a radial basis function neural network (RBFNN). The modified 7-level boost active-neutral-point-clamped inverter is operated like a SAPF, while an adaptive neuro-fuzzy inference system (ANFIIS) is used to tune the proportional-integral controller to control the DC-link voltage and RBFNN is used to process the extraction of harmonics and reference current. The presented method eliminates current harmonics while compensating for reactive power. Nevertheless, the RBFNN's dependence on the fuzzy K-means clustering algorithm for center localization during training may limit its effectiveness, particularly with complex datasets.

In [37], a single-frequency-decoupled (SFD) approach is suggested for reducing the harmonics while also enhancing the performance of the distributed systems. The approach is to enhance the traditional indirect extraction scheme, and the evenorder voltage harmonics are mitigated. A proportional-resonant (PR) controller is used. Reference [38] presents ANFIS, an Artificial Neural Network and Recurrent Neural Network, as methods for reducing harmonics and improving power factor in power distribution networks using SAPF. The main aim of the suggested technique is to improve the performance through minimizing the THD. In [39], the SAPF is used to satisfy the customer requirement of high quality supply through the reduction of harmonics. Reference [40] proposes a model reference adaptive system for eliminating the harmonics of the system. The hardware cost of the SAPF is minimized by using a DC voltage estimation method to reduce load and filter current sensors.

Recent work highlights as an important factor the power quality issue of the distributed systems. Some loads produce very high harmonic current which leads to significant distortion in the distribution network. This results in higher power losses and a reduced power factor. At the site of intersection where various users are connected to the network, distortion often occurs because of variable speed drives and large industrial converters. Therefore, recent harmonic mitigation approaches are used to reduce these effects which are

caused by power electronics and non-linear loads. Various methods are available, e.g., using active and passive filters, though selecting the best method is not straightforward. Some technologically advanced solutions offer definitive outcomes and with negligible negative effect in the isolated electrical system. Conversely, the performance of other simpler approaches is highly dependent on the condition of the system. These drawbacks have motivated this work.

III. Configuration of SAPF-connected PV System

Configuration of the SAPF-connected PV system is displayed in Fig. 1. Here, the half-bridge interleaved buck SAPF (HBIB-SAPF) is employed to reduce system harmonics. The proposed system is incorporated into three parts, i.e., power grid, non-linear load and HBIB-SAPF-tied PV system. The grid is represented by a 3-phase sinusoidal supply voltage behind a 3-phase R-L impedance network. A 3-phase full-bridge rectifier is connected parallel to the grid [41]–[43] and is used as the non-linear load. SAPF is formed by a 3-phase HBIB-converter through a PV source.

The HBIB-SAPF is incorporated with 3 single-phase dual buck power cells that are tied with a direct current capacitor. Two IGBTs, two diodes, and two coupling inductors are used for each cell. The filter current is smoothed by the interfacing inductors that connect the HBIB-SAPF to the grid at the point of convergence.

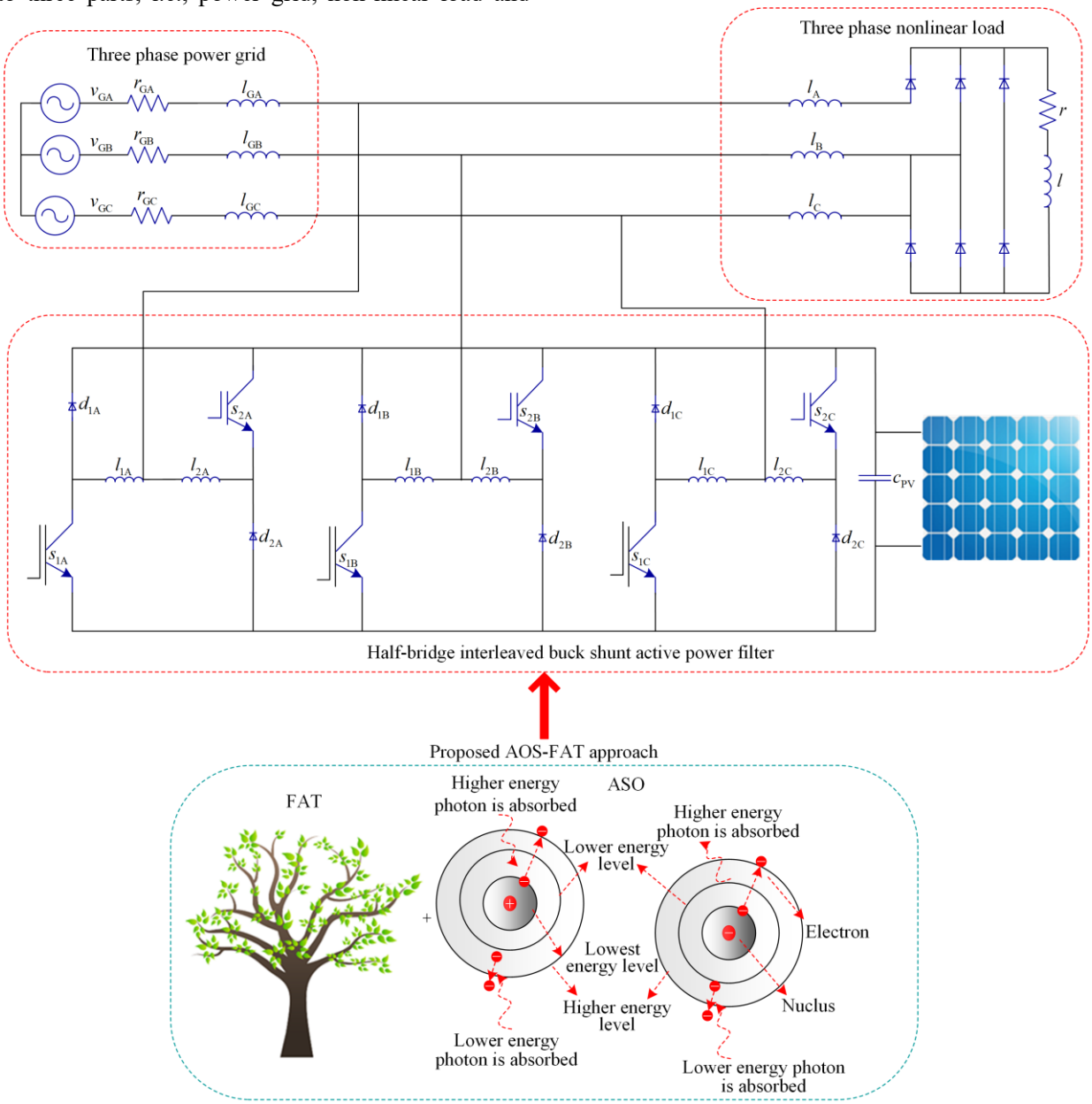

Fig. 1. Configuration of SAPF connected PV system.

A. Modelling of PV System

In general, a photovoltaic system has a DC-DC converter, a load, and a photovoltaic module [44]. The PV cells are placed in parallel or series to obtain a specific value of voltage and current from the PV module. The PV cell generates a PN junction that uses sunlight to generate photocurrent and operates as a diode. A circuit diagram of a single diode solar cell is portrayed in Fig. 2. As seen, the current source contains a resistor and a diode [45], [46]. The PV properties are mathematically expressed below.

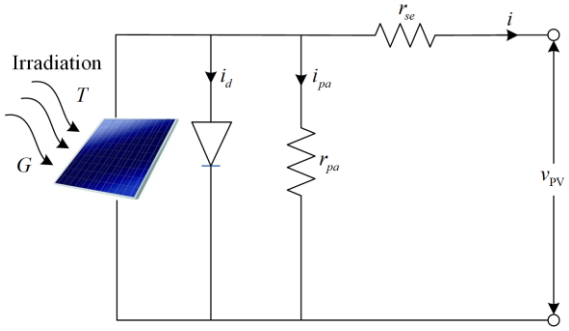

Fig. 2. Circuit model of a single diode solar cell.

The characteristic current of a PV cell is described by:

$$i = i_{\mathrm{PH}} - i_{\mathrm{Satu}}\left(\mathrm{e}^{\frac{v+iR_{\mathrm{S}}}{q_f v_{\mathrm{Ther}}}} - 1\right) \tag{1}$$

where i denotes the PV cell's output current; i_{PH} denotes the light generated current; v_{Ther} refers to the thermal voltage; iR_{s} is the product of the quality factor q_f and the series resistance R_{s}; and i_{Satu} is a constant representing the diode saturation current. The current created by light is proportional to the intensity of the light, computed as:

$$i_{\mathrm{PH}} = i_{\mathrm{Ther}}\frac{i_{\mathrm{PHo}}}{i_{to}} \tag{2}$$

where i_{Ther} is the standard light intensity; i_{PHo} refers to the light current created in an open circuit; and i_{to} is a constant.

$$i_O = i_{\mathrm{PH}} - i_{\mathrm{Satu}}\mathrm{e}^{\left(\frac{qV_{\mathrm{openc}}}{q_f v_{\mathrm{Thert}}}\right)} - \frac{V_{\mathrm{openc}}}{R_{\mathrm{ST}}} \tag{3}$$

where q indicates the elementary charge; V_{openc} indicates the open circuit voltage of the PV cell; i_O indicates the current saturation diode; and R_{ST} indicates the series resistance of the shunt diode in the PV cell. According to (3), the reverse saturation current is:

$$i_{\mathrm{Satu}} = \left(i_{\mathrm{PH}} - \frac{V_{\mathrm{openc}}}{R_{\mathrm{ST}}}\right)\mathrm{e}^{-\frac{-qV_{\mathrm{openc}}}{q_f v_{\mathrm{Thert}}}} \tag{4}$$

The saturation current is:

$$i_o = \left(\frac{i_{\mathrm{sc}}(R_{\mathrm{se}} + R_{\mathrm{sh}}) - V_{\mathrm{oc}}}{R_{\mathrm{sh}}}\right)\mathrm{e}^{\frac{-qV_{\mathrm{oc}}}{nv_t}} \tag{5}$$

where i_{sc} indicates the current used in a short circuit; R_{se} and R_{sh} indicate the shunt and series resistances, correspondingly. n indicates the ideality factor; V_{oc} denotes the open circuit voltage and v_i indicates the voltage at the knee of the diode characteristic curve. The maximum power point condition is applied and is calculated as:

$$i_{\mathrm{mpp}} = i_{\mathrm{PH}} - \left(\mathrm{e}^{\frac{q(V_{\mathrm{mpp}} + i_{\mathrm{mpp}}R_{\mathrm{SE}})}{q_f v_{\mathrm{Ther}}}} - 1\right) - \left(\frac{V_{\mathrm{mpp}} + i_{\mathrm{mpp}}R_{\mathrm{SE}}}{R_{\mathrm{ST}}}\right) \tag{6}$$

where v_{mpp} and I_{mpp} are the current and voltage at the MPP while R_{SE} is the shunt resistance at the MPP.

B. Modelling of DC-link Voltage

To guarantee appropriate current injection, the direct current-link voltage needs to be more than twice the peak grid voltage [47], i.e:

$$v_{\mathrm{PV,min}} \geqslant 2v_{\mathrm{GRID}} \tag{7}$$

where v_{GRID} represents the peak grid voltage [48]. The required DC-link capacitance is calculated by:

$$c_{\mathrm{PV}} = \frac{p_{\mathrm{PV}} / v_{\mathrm{PV}}}{2 \times f_{\mathrm{GRID}} \times \Delta v_{\mathrm{PV}}} \tag{8}$$

where power transmitted through the PV panel in MPP is expressed as p_{PV}; the DC-link voltage is indicated as v_{PV}; the ripple amplitude of the PV voltage is indicated as Δv_{PV}; and the grid angular frequency is indicated as f_{GRID}. Considering that the voltage of the grid is sinusoidal, it can be described as:

$$v_{\mathrm{GRID}J}(t) = V_{\mathrm{GRID}}\sin\left(f_{\mathrm{GRID}}T - \frac{2\pi}{3}(i-1)\right), \quad (J = A,B,C),(i = 1,2,3) \tag{9}$$

The load current is described by:

$$i_{\mathrm{LOAD}J}(T) = \sum_{H=1}^{\infty} i_{J,H}\sin(Hf_{\mathrm{GRID}}T + \phi_H), (J = A,B,C) \tag{10}$$

where the Hth harmonic load current component is $i_{\mathrm{LOAD}J}(T)$; the amplitude and phase are expressed as $i_{J,H}$ and ϕ_H, respectively.

IV. Control Structure of The Proposed HBIB-SAPF

Current and voltage control using the proposed approach is displayed in Fig. 3. Here, inner and outer loops are considered [49], where the outer loop is employed to control the voltage within the system and the inner loop is used to control the system current.

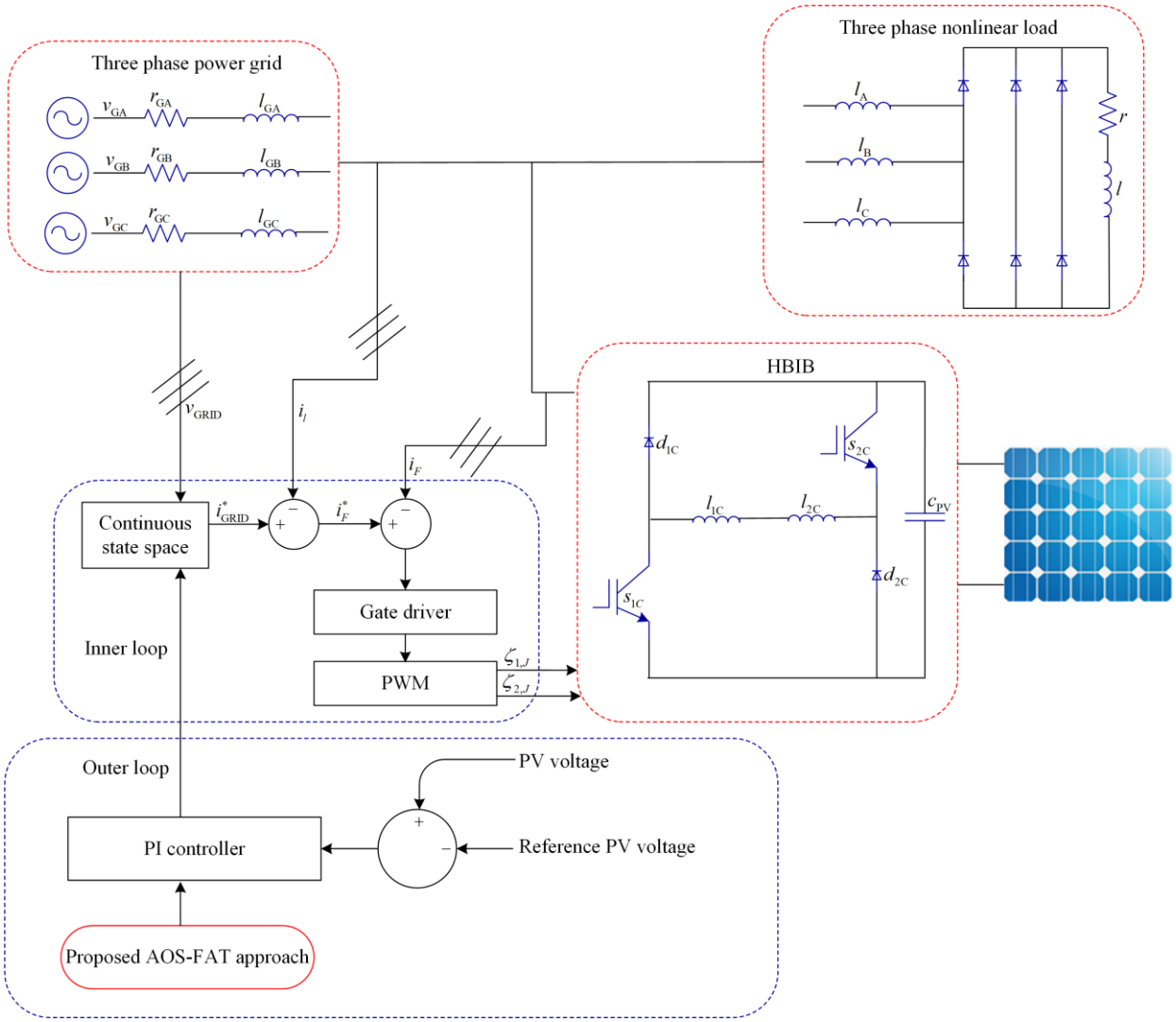

Fig. 3. Voltage and current control using proposed approach.

A. Modelling of HBIB Switches

The switches operate in accordance with current flow via the output filter i_{FJ}. If the filter current is positive then S_{1J} and d_{1J} are in operation, and if it is negative, then S_{2J} and d_{2J} are operational [50]. The HBIB converter switching signals are described by:

$$\zeta_{1J}=\begin{cases}1 & s_{1J}\text{ on};\ \ d_{1J}\text{ off}\\ 0 & s_{1J}\text{ off};\ \ d_{1J}\text{ on}\end{cases}$$
$$\zeta_{2J}=\begin{cases}1 & s_{2J}\text{ on};\ \ d_{2J}\text{ off}\\ 0 & s_{2J}\text{ off};\ \ d_{2J}\text{ on}\end{cases} \tag{11}$$

The switching function is defined based on filter current polarity, as:

$$\zeta_{3J}=\begin{cases}+1 & \text{when}\ \ i_{FJ}>0\\ -1 & \text{when}\ \ i_{FJ}<0\ (J=A,B,C)\end{cases} \tag{12}$$

The switched model uses Kirchhoff's laws, and is described by:

$$l\frac{\mathrm{d}i_{l1_J}}{\mathrm{d}t}=(v_{PJ}+v_{\mathrm{PV}_J}(2\zeta_{1J}-1))\zeta_{3J} \tag{13}$$

$$l\frac{\mathrm{d}i_{l2_J}}{\mathrm{d}t}=(v_{PJ}+v_{\mathrm{PV}_J}(2\zeta_{2J}-1))(1-\zeta_{3J}) \tag{14}$$

$$c_{\mathrm{PV}}\frac{\mathrm{d}v_{\mathrm{PV}}}{\mathrm{d}T}=(i_{\mathrm{PV}}-i_{L1_J}(2\zeta_{1J}-1))\zeta_{3J}+(i_{\mathrm{PV}}+i_{l2_J}(2\zeta_{2J}-1))(1-\zeta_{3J}) \tag{15}$$

where the inductance currents are denoted as i_{L1_J} and i_{l2_J}; current and voltage generated through the PV source is denoted as i_{PV} and v_{PV}; and the driving signal for the switches is denoted as $\zeta_{(1,2)J}$. When the switches are identical, $l_{1J}=l_{2J}=l$.

B. Modes of Operation of the HBIB-SAPF

Each dual buck power cell for the photovoltaic-assisted HBIB-SAPF converter may be expressed in terms of 4 state equations, where every mode is associated with a particular converter topology, as shown in

Fig. 4 [51]. As seen, in mode 1, the switch s_{1A} and inductor l_1 carry the current while the other components, e.g., d_{1A}, s_{2A}, d_{2A} are off. In mode 2, the diode d_{1A} and inductor l_1 carry the current while s_{1A}, s_{2A}, d_{2A} are off.

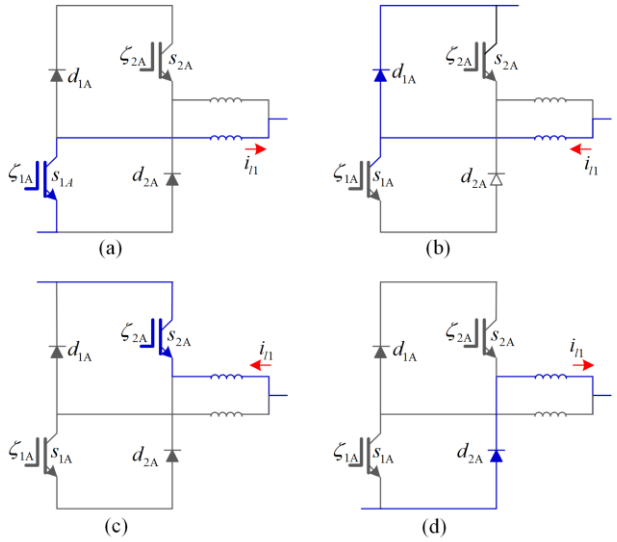

Fig. 4. Phase A operating mode of HBIB converter.

C. Modelling of Current Control Loop

The grid current must equal the reference signal to correct the 'current harmonics' and to obtain the power factor correction. Based on a specific grid voltage, this matching current processes the grid current in proportion and in phase. Hence, it is achieved by ensuring the filter current matches the reference current, computed by:

$$i_{FJ}^{*} = \chi v_{GRIDJ} - i_{LOADJ}, (J = A, B, C) \tag{16}$$

where the appropriate conductance for the amplitude of grid current is denoted as χ.

D. Modelling of Voltage Control Loop

It is used to guarantee the control of the DC-link voltage according to power balance between the PV panel and grid [52]–[54]. Based on the reference signal of the PV, its voltage is controlled and the control signal is generated. The proposed technique is used to regulate the system voltage.

V. Proposed Approach for Harmonic Reduction

This paper proposes an intelligent AOS-FAT technique to mitigating the system harmonics. The proposed grid-connected PV system is incorporated with SAPF using HBIB. The key purpose of the proposed method is to reduce the harmonics and reactive power that are due to non-linear load, to extract maximum power of PV, and to regulate the DC voltage. Initially, the AOS method is used to optimize datasets related to key electrical parameters, considering load variation and PV characteristics. Next, the FAT approach generates optimal control signals based on the optimized datasets. These control signals are then employed to eliminate harmonic distortion in the distribution system. Components used include data sources, control hardware, SAPF, and PV systems, collectively enhancing power quality and efficient renewable energy utilization. AOS-FAT effectively reduces harmonic distortions and stabilizes voltage levels in distribution systems, ensuring a more reliable and cleaner power supply. The technique optimizes control signals for PV systems, maximizing the utilization of renewable energy sources and promoting sustainable power generation. A limitation of the AOS-FAT technique is its adaptability to emerging technologies and evolving energy grid architectures. The following subsections provide a detailed explanation of the proposed methodology.

A. Proposed AOS Approach for Control Signal Generation

AOS is a meta-heuristic optimization method depending on the nucleus of an atom and guided by the attention rules of quantum physics [55]. The waves formed by the motion of electrons are combined in the unknown location as an alternative to orbiting in fixed pathways among the nucleus. The orbitals are definite in terms of electron placement probability, while the mathematical concept for defining the probability of any electron's particular location surrounding the atom nucleus is used. Based on the time, electrons instantly change positions and operate like a cloud of charge. In this paper, AOS is used to reduce the error of the system. The stepwise procedure of the proposed method is explained in the following steps.

1) Initiation

Start the input-parameters, such as PV voltage, DC current, iteration boundaries and voltage.

2) Random Generation

After initialization, the input-parameters are generated in matrix form at random, calculated as:

$$\boldsymbol{r}_X = \begin{bmatrix} v_{PV}^{11}(t) & v_{PV}^{12}(t) & \cdots & v_{PV}^{1n}(t) \\ v_{PV}^{21}(t) & v_{PV}^{22}(t) & \cdots & v_{PV}^{2n}(t) \\ \vdots & \vdots & & \vdots \\ v_{PV}^{m1}(t) & v_{PV}^{m2}(t) & \cdots & v_{PV}^{mn}(t) \end{bmatrix} \tag{17}$$

3) Evaluate the Fitness for Initial Solution

The fitness is determined by the objective function, given as:

$$F(X) = \min\left[E_m(t)\right] \tag{18}$$

$$E_m(t) = v_{PV}(t) - v_{PV}^{*}(t) \tag{19}$$

4) Compute the Binding State and Energy

The energy and binding state are calculated using:

$$B_s^K = \frac{\sum_{j=1}^{c} x_j^K}{c}, \begin{cases} j = 1,2,\ldots,c \\ K = 1,2,\ldots,n \end{cases} \tag{20}$$

$$B_e^K = \frac{\sum_{j=1}^{c} E_j^K}{c}, \begin{cases} j = 1,2,\ldots,c \\ K = 1,2,\ldots,n \end{cases} \tag{21}$$

where B_s^K is the binding state; B_e^K is the binding energy; and c implies candidates in the kth hypothetical layer. The optimal solution is determined by (20) and (21).

5) Create Random Parameters

Randomly create the random-parameters, e.g., ρ, μ, and υ.

6) Measure Photon Rate

The photon rate, which is dependent on the emission and absorption of electrons, is used to compare various interactions. When the random-parameter ρ is greater than or equal to the photon rate, the electron mobility is dependent on the emission and absorption. Conversely, when ρ is smaller than that rate, the particle interaction determines the electron mobility.

$$x_{j+1}^K = x_j^K + \text{Rand}_j \tag{22}$$

where Rand_j are uniformly distributed random numbers between [0, 1].

7) The Energy Level and Binding Energy Are Compared

If the energy level is higher than the binding energy, the position is updated as follows:

$$x_{j+1}^K = x_j^K + \frac{\rho_j \times (\mu_j \times l_e - \upsilon_j \times B_s)}{K} \tag{23}$$

If the energy level crosses the binding energy threshold, the position is modified as follows:

$$x_{j+1}^K = x_j^K + \rho_j \times (\mu_j \times l_e - \upsilon_j \times B_s^K) \tag{24}$$

The binding energy and state are determined from (23) and (24), while the comparison results are used to update the settings.

8) Finding the Best Global Solution

The goal is to find the optimal global solution that minimizes system errors and maximizes performance. This solution is determined based on the binding energy and state.

9) Examine Termination Criterion

If the termination criterion is satisfied, the process is terminated; if not, the process is repeated.

B. FAT Based Prediction of Control Signal

The FAT algorithm is an improvement on the artificial tree algorithm that takes inspiration from the way trees grow—that is, how organic matter is transported from the leaves to the roots and moisture is transferred from the roots to the leaves. The FAT approach [56] is established depending on the moisture transmission and organic matters. The forward process updating in this algorithm is based on branch territory, fitness value, maximal search number, and crowded tolerance. The backward updating is accomplished using the self-proportion, random, and dispersion propagation operators. The thinnest branch provides the best solution. The design of FAT is displayed in Fig. 5. In this study, FAT is used to determine the optimum job of the machine. The stepwise procedure of FAT is:

1) Input and Training

In step 1, $x(t)$ is the input, and the output Z is made into a FAT classification by using the training set, given as:

$$x_b = (x_{b1}, x_{b2}, \cdots, x_{bd}) \tag{25}$$

where d is the dimension; and b is the branch.The goal is to classify and predict control signals based on this training data.

2) Count Branches

Count the number of branches in the branch population after examining the first system population.

3) Fitness Calculation

Calculate fitness *Fit* for each branch using input data and target output:

$$Fit = \min(Error) \tag{26}$$

4) Determine Crowd Distance

Calculate the crowd distance by dividing the branch's territory:

$$T_{\text{branch}} = 2l(1 + Fit(x_F)) \tag{27}$$

$$d_{IJ} = \left\| x_1 - x_J \right\| \tag{28}$$

This crowd distance establishes the gap between the branches.

5) Apply Crossover Operator

The crossover operator is applied to create a new population of branches. This operator combines characteristics of existing branches to potentially improve performance, as:

$$x_{0J} = x_{IJ} + R((-1,1) \times (T_{\text{branch}} / 2)) \tag{29}$$

6) Select the Population of the Best Branch

Choose the best branch population and update system parameters based on fitness:

$$l_{\max,I} = n \times Fit(x_I) + n \tag{30}$$

Then, the optimal system parameter is updated.

7) Select the First Branch's Population for the Feedback Procedure

The population of the first branch for the feedback process is chosen as:

$$X_{\text{new}} = r \text{ choose}(X, \frac{\text{new selcted branch}}{X}) \tag{31}$$

where the population of the chosen branch and branch population are X_{new} and X, respectively. Then check the territory and crowded distance.

8) In the Feedback Process

If the branch territory is greater than or equal to the crowded tolerance, then update the branch value by

using the self-propagating operator. Thus, the value of islanded mode is:

$$X_N = X_i + (R\ (0,1) \times X_{bst} - R\ (0,1) \times X_i) \times a \quad (32)$$

where a is a constant related to the golden section theory for enhancing the system efficacy.

9) Perform the Operator of Dispersive-propagation

In the feedback method, if the branch territory is greater than or equal to the crowded tolerance, the value of branch i is updated using the dispersive propagation operator, as:

$$y_{oj} = y_{ij} + Rand(-1,1) \times (V_i / 2) \times a \quad (33)$$

$$y_{tj} = y_{ij} - Rand(0,1) \times y_{oj} \quad (34)$$

where the updated branch element (X_O, X_t) is expressed by y_{oj} and y_{ij}, while $j = 0,1,2 \ldots m$.

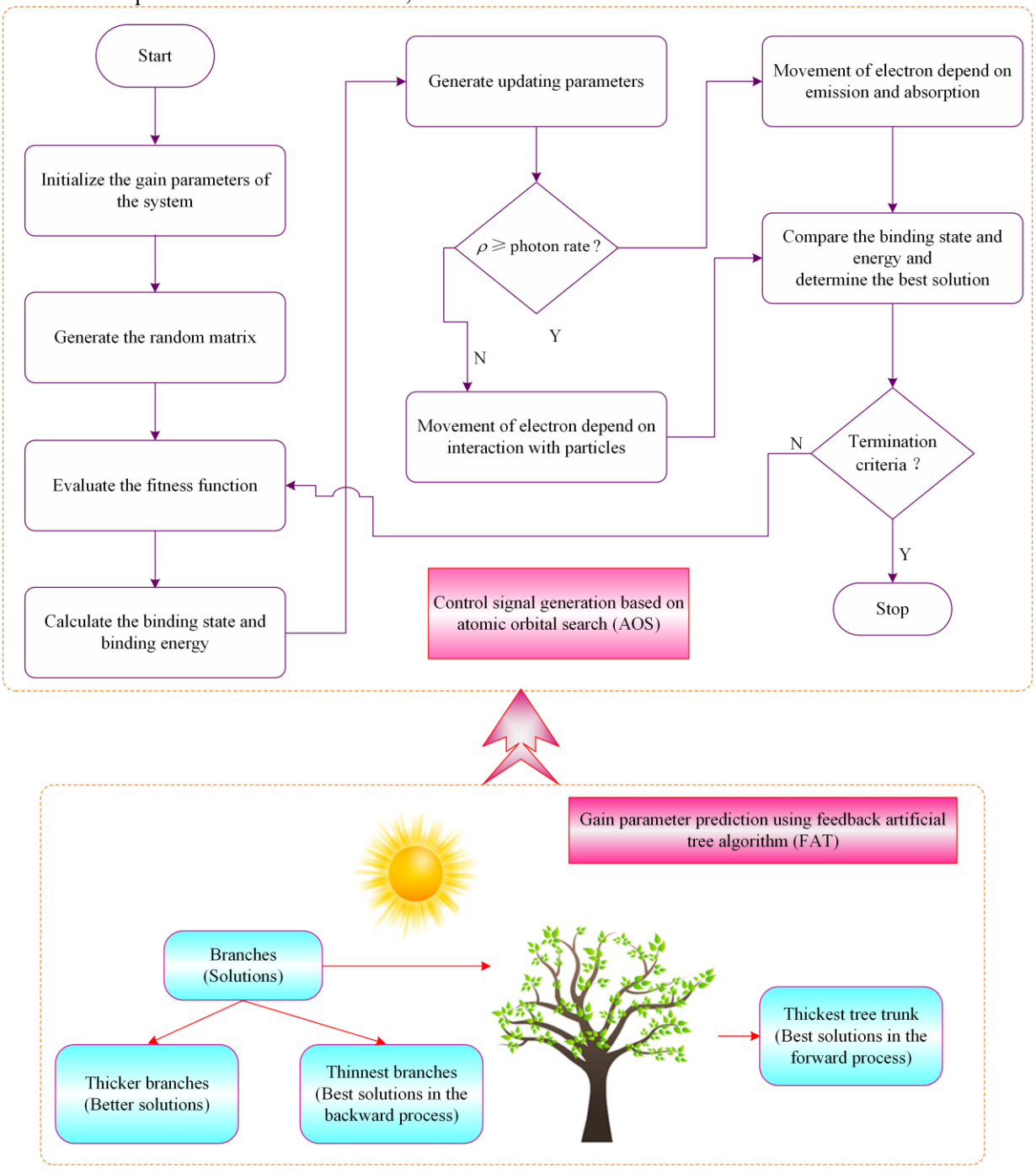

Fig. 5. Flow chart of the FAT-AOS approach.

Then update the procedure, combine the old and new populations, and build a new population using this combination. Continue until the process reaches the maximum iteration. FAT is well trained to forecast the control signal of SAPF using the above steps. Figure 6 depicts the flowchart of the FAT-AOS approach. In

summary, these steps describe how the proposed AOS and FAT algorithms work together to optimize a grid-connected PV system with SAPF. The proposed SOS-FAT focuses on reducing harmonics, improving power extraction from PV sources, and regulating the DC voltage.

VI. Results and Discussion

Here the outcomes of simulation are presented to demonstrate the performance of the proposed approach in enhancing the power quality and increasing the maximum power of the PV system. The whole system including the designed controllers is simulated and the performance is analyzed in the MATLAB platform. The proposed approach is examined for four cases: without PV module, standard climatic conditions, irradiation variation condition, and temperature variation condition. Then, the proposed approach's performance is constrasted with various existing approaches. The non-linear load presented in the system produces harmonics as described in Fig. 6. From the load current, it is clear that the harmonics of the system are high with a THD of 39%.

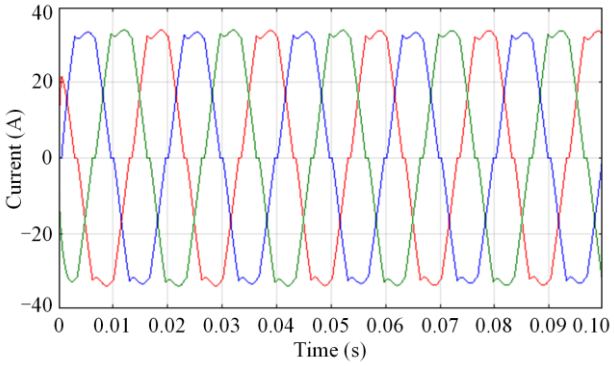

Fig. 6. Analysis of load current.

1) Performance Analyses of the Proposed Approach without the PV Module

Here, the performance of the proposed strategy in the PV disconnection condition is analyzed. Hence, only the SAPF is connected in the proposed method, the system is working properly and the total demand of load is satisfied by the grid only.

Figure 7 shows the grid voltage and current. As seen, the grid current is sinusoidal and is in phase with the grid voltage, confirming that the compensation of harmonics and reactive power is well performed. Analyses of the grid power, PV power, and load are shown in Fig. 8 (a), while Fig. 8 (b) shows the DC-link voltage. As seen, the PV power is zero, and the load power is satisfied by the grid. The DC-link voltage in Fig. 8 (b) shows that it remains constant at 800 V, ensuring system stability throughout the simulation period. Figure 9 shows the analysis of the control signal using the proposed method. This contributes to the smooth operation of the system in these conditions.

In Case 1, the absence of a PV module does not hinder the system's ability to meet load demand effectively. The grid voltage and current remain synchronized, eliminating undesired harmonics and reactive power.

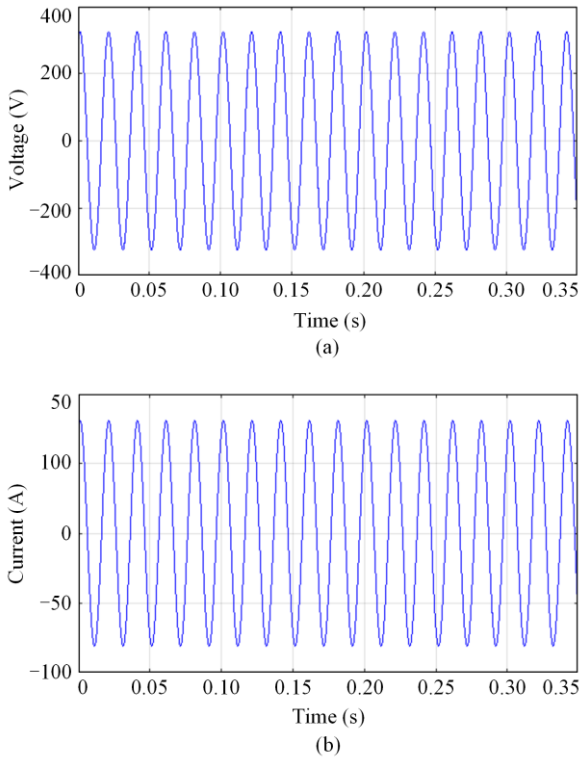

Fig. 7. Analyses of grid. (a) Voltage. (b) Current.

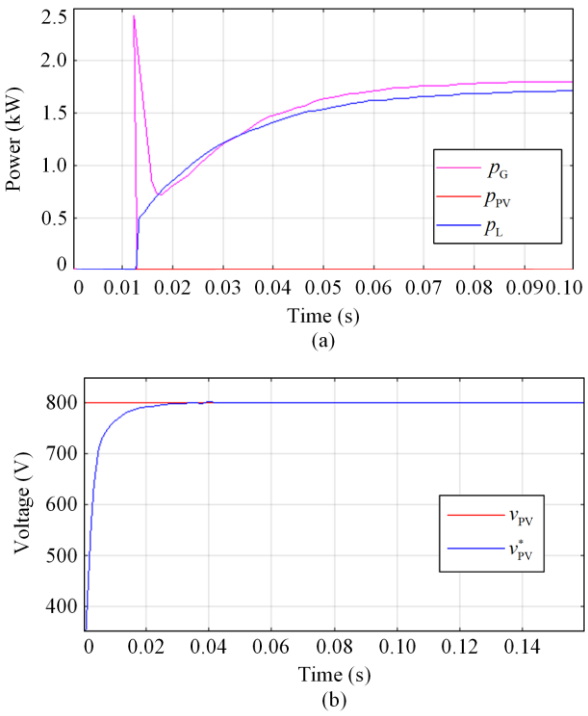

Fig. 8. Evaluations of index. (a) Power of grid, PV power, and load. (b) DC link voltage.

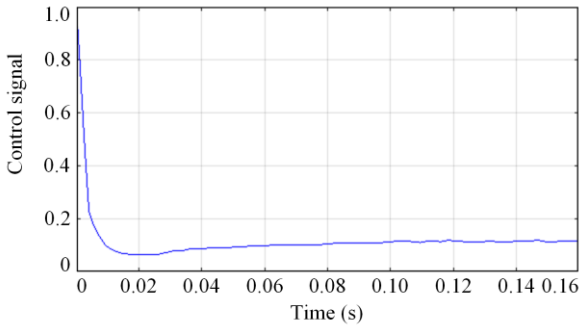

Fig. 9. Analyses of control signal using proposed method.

2) Performance Analyses of the Proposed Approach in Standard Climate Conditions

Standard climatic conditions are characterized by a constant temperature of 25 °C. The PV voltage and control signals are displayed in Figs. 10 (a) and (b), respectively. As seen, the PV voltage remains stable at approximately 815 V after an initial transient, with minimal fluctuation. The control signal in Fig. 10 (b) shows that the average of the signal reaches its steady-state value after a short transient.

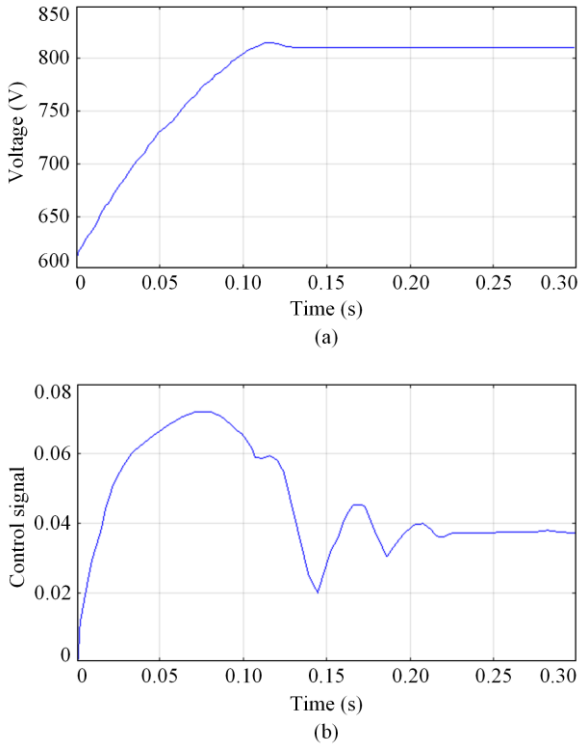

Fig. 10. Investigation of grid. (a) PV voltage. (b) Control signal.

Figure 11 (a) illustrates the power of PV, load and grid. It is evident that a portion of the power needed by the non-linear load is supplied by the PV, while the rest is met by the grid. The PV power starts at 9 kW and increases to 12 kW at 0.1 s, and then is maintained at 12 kW thereafter. Figure 11 (b) illustrates the current of the filter. As seen, the filter effectively mitigates harmonic distortions, with a filter current magnitude of around 25 A.

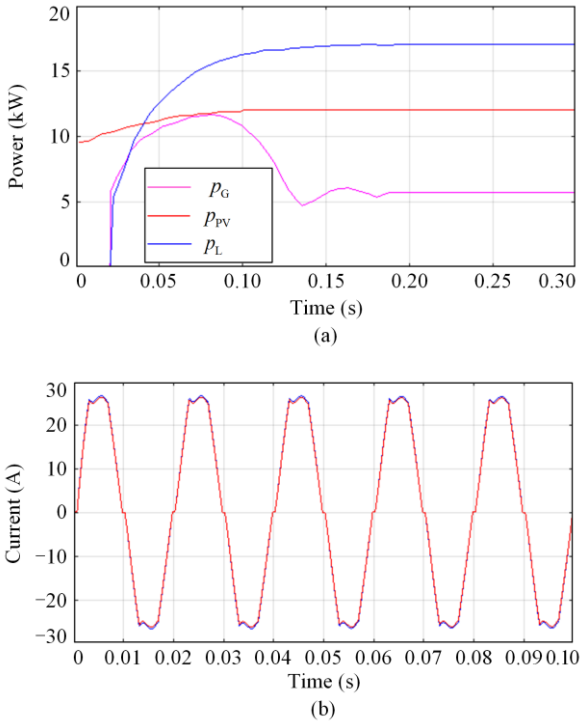

Fig . 11. Investigation of grid. (a) Power of PV, load and grid. (b) Filter current.

The three-phase grid current is displayed in Fig. 12. As seen, its magnitude is around 25 A between 0 to 0.1 s, and then reduces to 20 A between 0.1 s to 0.35 s. From the grid current, it can be seen that the undesired harmonics are eliminated. The phase a grid voltage and current are displayed in Figs. 13 (a) and (b), respectively. As seen, the voltage magnitude is 300 V from 0 to 0.35 s, while the current magnitude is 180 A between 0 to 0.1 s and then decreases to 150 A between 0.1 s to 0.35 s. From Fig. 13, it is seen that the voltage and current harmonics are corrected. The power factor displayed in Fig. 14 shows that the correction of the power factor is performed effectively, while the near-unity power factor indicates an improvement in power quality.

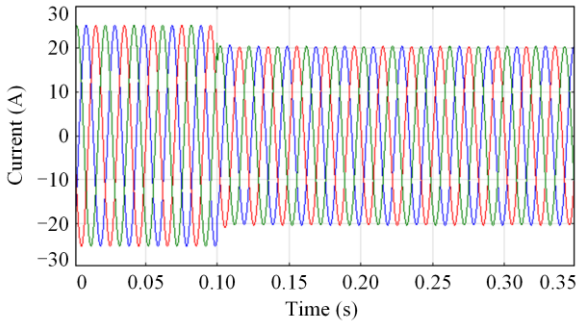

Fig. 12. Analyses of the three-phases grid current (i_{grid}, ABC).

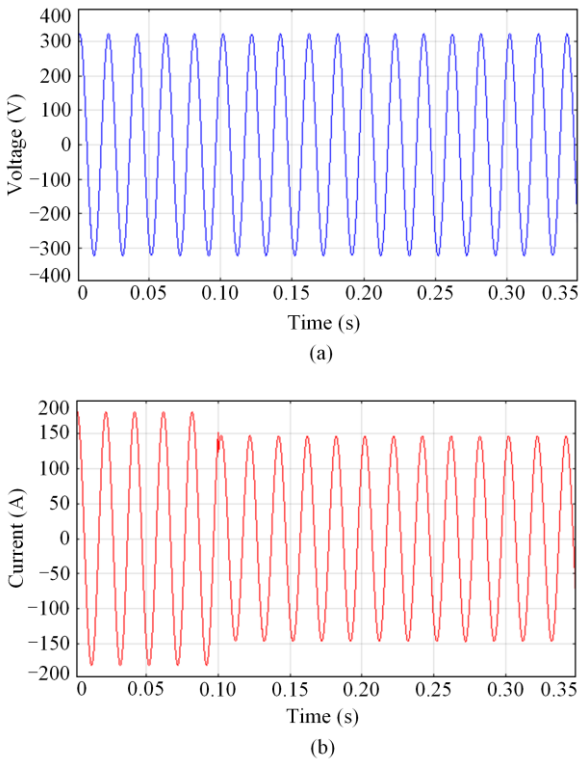

Fig. 13. Investigation of grid. (a) Voltage. (b) Current.

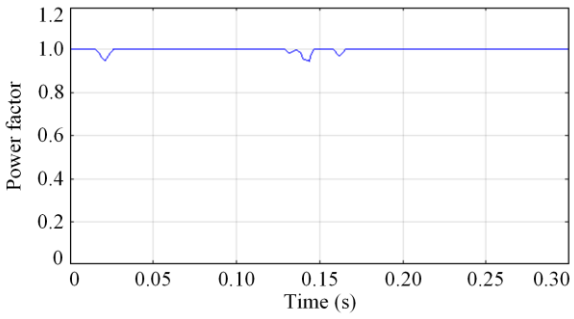

Fig. 14. Evaluations of power factor.

In Case 2, in standard climatic conditions, the proposed approach demonstrates robust performance. It effectively corrects voltage and current harmonics, and leads to a near-unity power factor. The system maintains stable operation, ensuring high-quality power transfer to the load.

3) Performance Analyses of the Proposed Method in an Irradiance Variation Condition

Here solar irradiance and power of grid, PV and load are displayed in Fig. 15. As seen from Fig. 15 (a), the solar irradiance changes from 1 kW/m^2 to 0.8 kW/m^2 at 0.35 s, and then ramps up between 0.65 s to 0.7 s to 0.9 kW/m^2. Figure 15 (b) shows the power of PV, grid and load. As seen, the load power remains constant at 1.75 kW from 0.1 s to 1.1 s, while the PV power starts at 1.25 kW between 0.1 s to 0.35 s, reduces to 0.9 kW from 0.35 s to 0.65 s, and then remains constant at 1.2 kW from 0.7 s to 1.1 s.

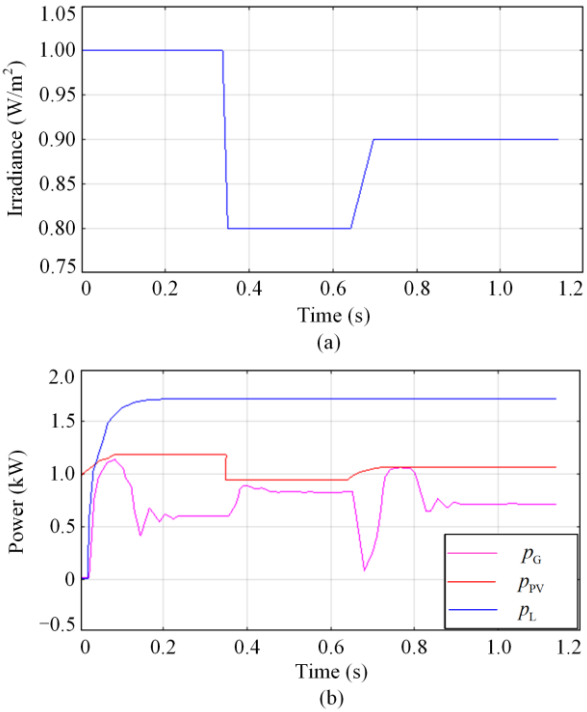

Fig. 15. Analyses of grid. (a) Solar irradiance. (b) Power of PV, grid and load.

Figures 16 (a) and (b) display the PV voltage and control signal respectively, based on the proposed approach. As seen, the PV voltage closely tracks its reference with the maximum voltage being 820 V, ensuring a stable DC voltage. From Fig. 16(b), it is seen that the control signal reaches the value of steady-state after every irradiation change. The currents of the filter and the three-phase grid are shown in Figs. 17 (a) and (b), respectively. As seen, the filter current accurately tracks its reference, effectively mitigating harmonic distortions. The grid current remains sinusoidal throughout the simulation, as displayed in Fig. 17 (b), further demonstrating the effective elimination of undesired harmonics. The grid voltage and current are displayed in Fig. 18. As seen, despite the variation in solar irradiance, the current and voltage remain in phase, confirming effective harmonic and reactive compensation. The analysis of power factor depicted in Fig. 19 also shows near unit power factor.

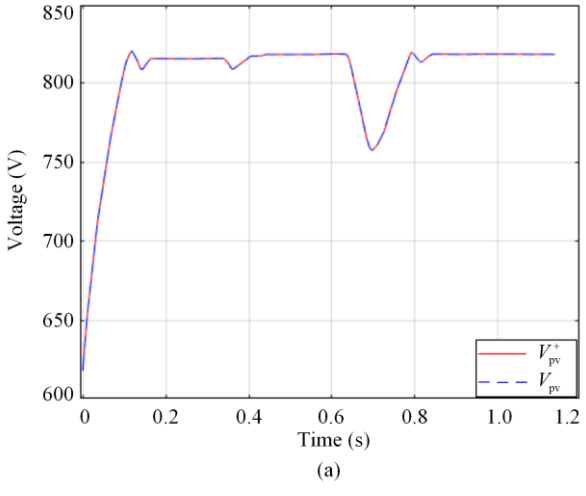

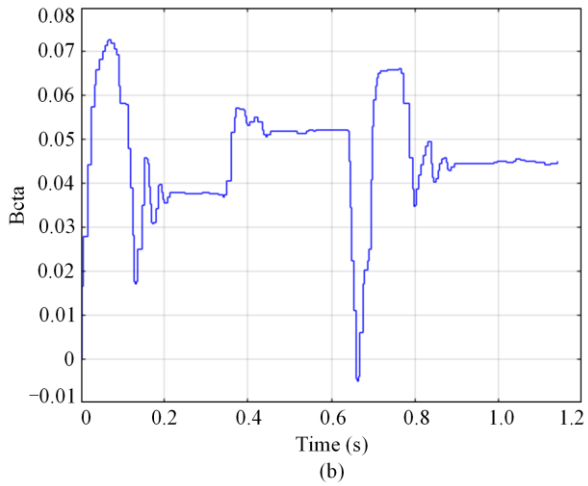

Fig. 16. Analyses of grid. (a) PV voltage. (b) Control signal based on proposed approach.

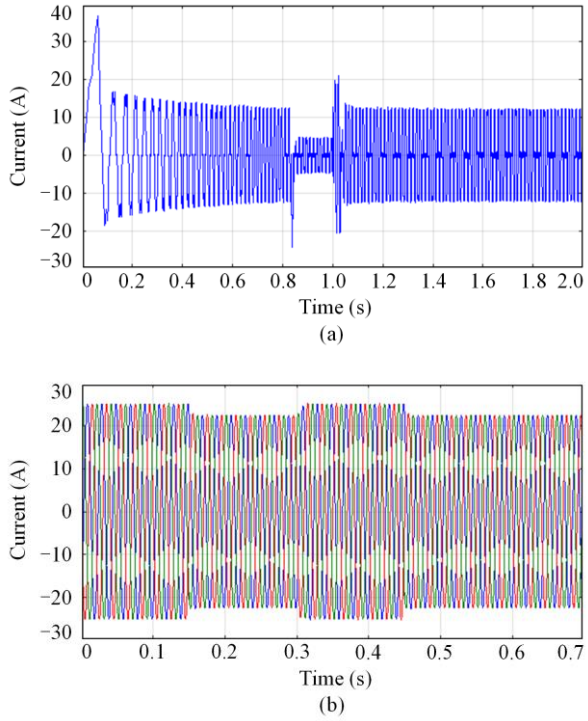

Fig. 17. Analyses the current . (a) Filter. (b) Three-phase grid.

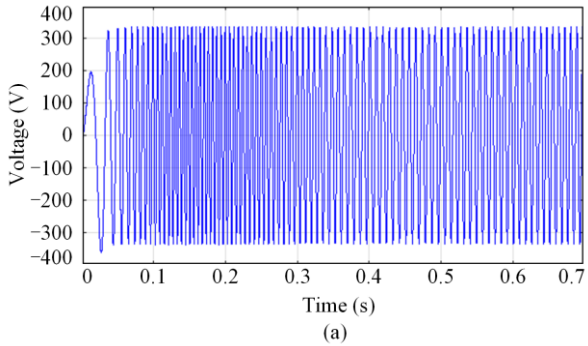

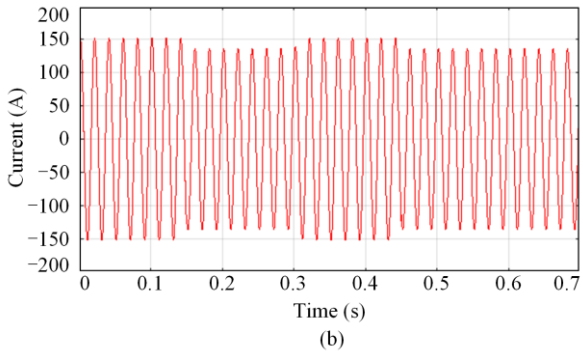

Fig. 18. Analyses of grid. (a) Voltage. (b) Current.

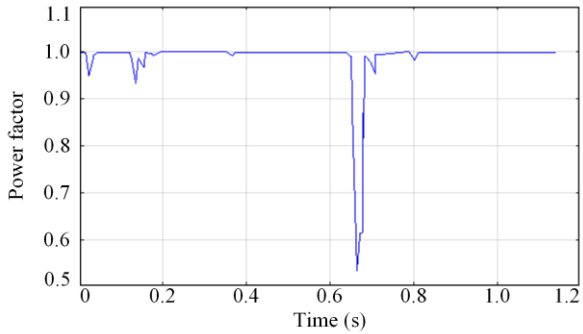

Fig. 19. Analyses of power factor.

Case 3 reveals that the proposed methodology effectively adapts to varying solar irradiance conditions, maintaining stable PV voltage and control signals. Power generation aligns with irradiance fluctuations, with clean grid current. The power factor remains near unity, contributing to improved power quality.

4) Performance of the Proposed Method Under Temperature Variation Condition

The changing of temperature in this case is illustrated in Fig. 20 (a). As seen, at the beginning of the simulation (0 to 0.3 s), the temperature is 25 °C. It increases to 40 °C from 0.3 s to 0.65 s, and then gradually decreases to 20 °C from 0.75 s to 1 s. The power of the PV, grid and load are shown in Fig. 20 (b). As can be seen, the load power remains constant at 17 kW from 0.1 s to 1 s, while the PV power starts at 12 kW at 0.1 s and remains stable at this level during the simulation. This demonstrates the system's ability to maintain power generation as the temperature changes.

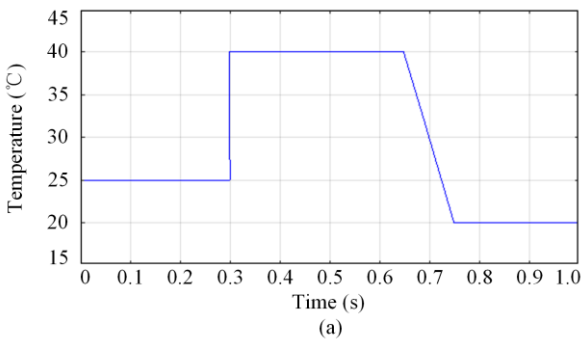

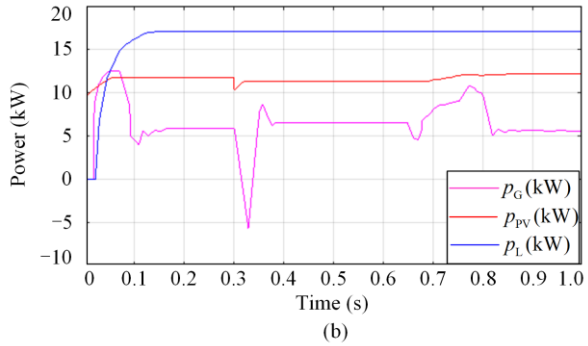

Fig. 20. Analyses of grid. (a) Temperature. (b) Power of photovoltaic, grid and load.

Figure 21 (a) shows that the PV voltage varies according to the varying temperature condition of the PV. Fig. 21 (b) shows the control signal generated using the proposed approach. As seen, the control signal reaches a new steady-state value after each change in temperature condition, ensuring efficient operation in response to temperature variation. Figure 22 (a) illustrates the performance of the filter current, which accurately tracks its reference, effectively mitigating harmonic distortions. From Fig. 22 (b), the grid current remains sinusoidal throughout the simulation, demonstrating the effective elimination of undesired harmonics.

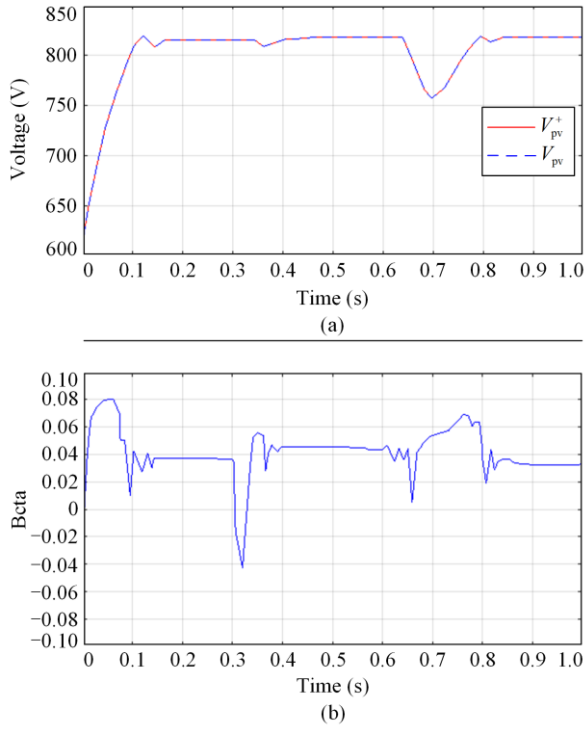

Fig. 21. Analyses of grid. (a) PV voltage. (b) Control signal based on proposed method.

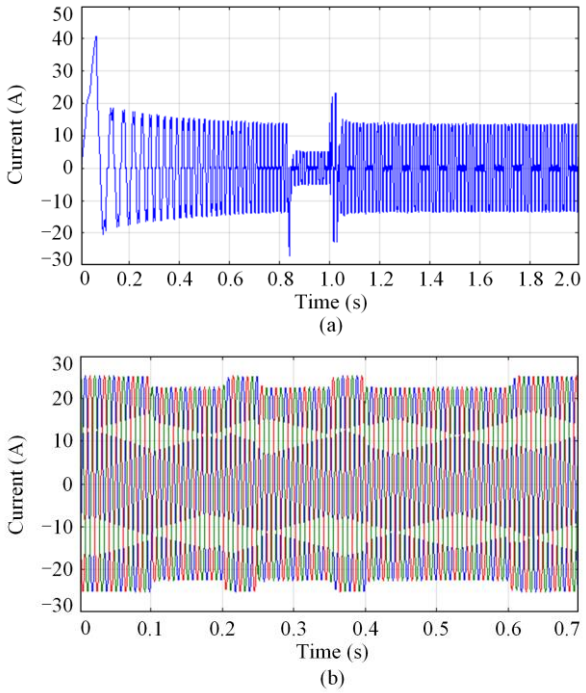

Fig. 22. Analyses of the current. (a) Filter. (b) Three-phase grid.

Figure 23 displays the grid voltage and current. As can be seen, despite the variation in temperature, the current and voltage remain in phase, confirming effective reactive current compensation. Figure 24 further shows that the correction of the power factor is performed effectively. This demonstrates improvement in power quality, especially during temperature variations.

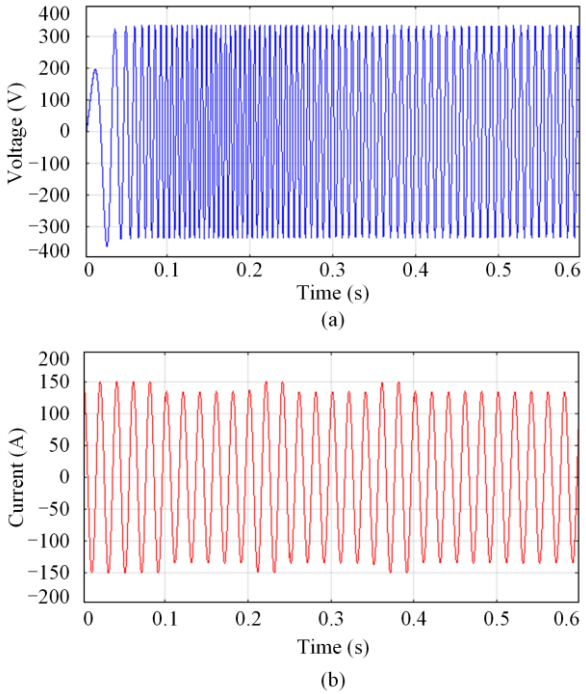

Fig. 23. Evaluations of grid. (a) Voltage. (b) Current.

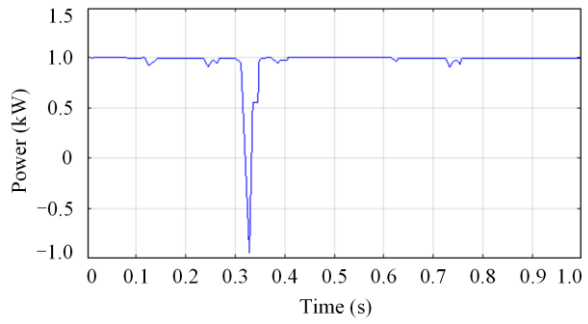

Fig. 24. Analyses of power factor.

In Case 4, the results indicate that the system effectively adapts to temperature changes, maintaining stable PV voltage, control signals, and power quality.

Analysis of THD is displayed in Fig. 25. The THD before the SAPF connection is 40%. After SAPF connecting with an irradiance of 800 W/m^2, the THD becomes 1.1 %, and for irradiance of 900 W/m^2, the THD is 1.34 %. Hence, THD is reduced significantly using the SAPF with the proposed approach. Figure 26 illustrates the comparison of THD with the proposed and existing methods.

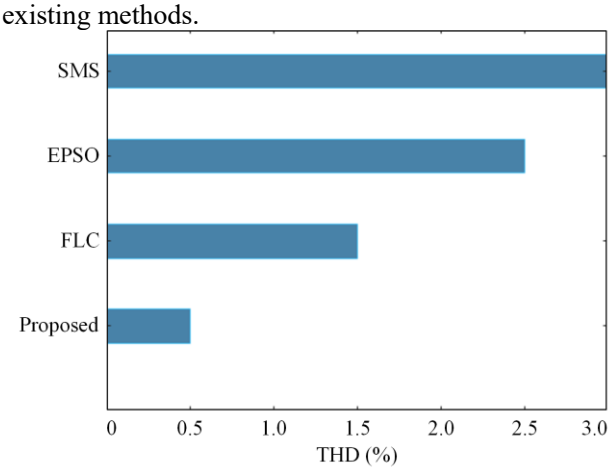

Fig. 25. Analysis of THD.

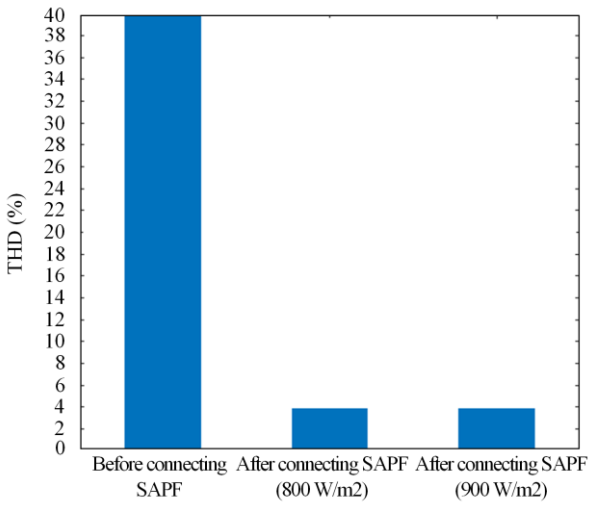

Fig. 26. THD in comparison to proposed and current approaches.

As seen, the proposed method results in 1.1 % THD, compared to 2% for FLC, 2.2% for EPSO, and 2.87% for the SMC approach.

The findings highlight the strength of the proposed method in various operational scenarios. Particularly, the SAPF shows its effectiveness in maintaining power quality by mitigating harmonic distortion and ensuring smooth grid interaction. The comparison with existing approaches, such as FLC, EPSO, and SMC, highlights the superiority of the proposed method, with significantly lower THD. This highlights the practicality and effectiveness of the proposed methodology in improving PQ.

ACKNOWLEDGMENT

Not Applicable.

AUTHORS' CONTRIBUTIONS

B. Kiruthiga: carry out the additional results based on the validation of the proposed technique and other techniques. R. Karthick: enhance the Abstract and conclusion part with main research findings and contribution of the proposed work. I. Manju: draw the figures with higher resolution and pasted them in the manuscript. Krishnaveni Kondreddi: carry out the minor typological mistakes and grammatical edits, English language correction throughout the manuscript. All authors have read and agreed to the published version of the manuscript.

FUNDING

Not Applicable.

AVAILABILITY OF DATA AND MATERIALS

Not Applicable.

DECLARATIONS

Competing interests: The authors declare that they have no known competing financial interests or personal relationships that could have appeared to influence the work reported in this article.

AUTHORS' INFORMATION

B. Kiruthiga received a B.E degree in instrumentation and control from Sethu Institute of Technology, Kariapatti affiliated to Madurai Kamaraj University in 2004. M.E degree in power electronics and drives from Pannai College of Engineering, Sivagangai affiliated to Anna University, Chennai in 2014 and Ph.D Degree in Electrical engineering from Anna University, Chennai in 2021. Her research interests include power quality, power electronics and renewable energy sources.

R. Karthick has undergone his B.E (ECE) in PTR College of Engineering and Technology, Madurai and done his postgraduate M.E (communication systems) in Sri Sairam Engineering College, Chennai. He has obtained his doctorate from Bharath University, Chennai. He has more than a decade of academic experience in the field of biomedical engineering, CMOS VLSI and testing.

I. Manju obtained her bachelor's degree (1996) in electronics and communication engineering with first class from Bharathidasan University, Tamil Nadu. She obtained her master's degree (2006) in VLSI design with first class & distinction from RMK Engineering College, Anna University, Chennai, Tamilnadu. She completed his doctoral degree (2017) in the area of VLSI design from Anna University, Chennai, Tamilnadu, India. He has 23+ years of teaching and research experience. She has published 30 papers in international journals, international and national conferences. Her research interests include VLSI signal processing, image processing, robotics, RPA and e-mobility.

Krishnaveni Kondreddi completed her B.Tech from Nagarjuna University in1992, M.S (DLPD) from BITS, Pilani in 1996, and M.Tech from JNTU, Hyderabad, INDIA in 2002. She is awarded Ph.D in electrical engineering in the area of flexible AC transmission systems from JNTU, Hyderabad in April 2009. Currently, she is working as professor in the EEE department of CBIT(A), Hyderabad. Her research interests include power electronics, FACTS and applications of power electronics to renewable energy systems.

REFERENCES

[1] N. H. A. Kahar and A. F. Zobaa, "Application of mixed integer distributed ant colony optimization to the design of undamped single-tuned passive filters based harmonics mitigation," *Swarm and Evolutionary Computation*, vol. 44, no. 1, pp. 187-199, Jan. 2019.

[2] F. Belloni, R. Chiumeo, and C. Gandolfi, "Shunt active power filter with selective harmonics compensation for LV distribution grid," In *International Conference on Renewable Energy and Power Quality*, Jan. 2015, pp. 1-10.

[3] K. Jyothi and R. B. Dubey, "Minimizing non-processing energy consumption/total weighted tardiness & earliness, and makespan into typical production scheduling model-the job shop scheduling problem," *Journal of Intelligent & Fuzzy Systems*, *(Preprint)*, vol. 1, no. 1, pp. 1-23, Jan. 2023.

[4] R. Arivalahan, S. Venkatesh, and T. Vinoth, "An effective speed regulation of brushless DC motor using hybrid approach," *Advances in Engineering Software*, vol. 174, no. 1, Jan. 2022.

[5] M. B. Latran, A. Teke, and Y. Yoldaş, "Mitigation of power quality problems using distribution static synchronous compensator: a comprehensive review," *IET Power Electronics*, vol. 8, no. 7, pp. 1312-1328, Jul. 2015.

[6] P. P. Biswas, P. N. Suganthan, and G. A. Amaratunga, "Minimizing harmonic distortion in power system with optimal design of hybrid active power filter using differential evolution," *Applied Soft Computing*, vol. 61, pp. 486-496, 2017.

[7] P. Rajesh, F. H. Shajin, and G. Kannayeram, "A novel intelligent technique for energy management in smart home using internet of things," *Applied Soft Computing*, vol. 128, no. 1, pp. 109442, Jan. 2022.

[8] H. Buch and I. N. Trivedi, "An efficient adaptive moth flame optimization algorithm for solving large-scale optimal power flow problem with POZ, multifuel and valve-point loading effect," *Iranian Journal of Science and Technology*, *Transactions of Electrical Engineering*, vol. 43, pp. 1031-1051, 2019.

[9] R. Santhi and A. Srinivasan, "An efficient AOA-RERNN control approach for a non-isolated quasi-Z-source novel multilevel inverter based grid connected PV system," *Energy*, vol. 263, no. 1, pp. 125492, Jan. 2023.

[10] S. Echalih, A. Abouloifa, and I. Lachkar *et al*., "A cascaded controller for a grid-tied photovoltaic system with three-phase half-bridge interleaved buck shunt active power filter: hybrid control strategy and fuzzy logic approach," *IEEE Journal on Emerging and Selected Topics in Circuits and Systems*, vol. 12, no. 1, pp. 320-330, Jan. 2022.

[11] M. Cerrada, G. Zurita, and D. Cabrera *et al*., "Fault diagnosis in spur gears based on genetic algorithm and random forest," *Mechanical Systems and Signal Processing*, vol. 70, pp. 87-103, 2016.

[12] F. H. Shajin, P. Rajesh, and M. R. Raja, "An efficient VLSI architecture for fast motion estimation exploiting zero motion prejudgment technique and a new quadrant-based search algorithm in HEVC," *Circuits*, *Systems*, *and Signal Processing*, vol.1, no. 1, pp. 1-24, Jan. 2022.

[13] S. R. Das, P. K. Ray, and A. Mohanty, "Improvement in power quality using hybrid power filters based on RLS algorithm," *Energy Procedia*, vol. 138, pp. 723-728, 2017.

[14] M. A. Elaziz, A. A. Ewees, and R. A. Ibrahim *et al*., "Opposition-based moth-flame optimization improved by differential evolution for feature selection," *Mathematics and Computers in Simulation*, vol. 168, pp. 48-75, 2020.

[15] M. R. Jannesar, A. Sedighi, and M. Savaghebi *et al*., "Optimal placement, sizing, and daily charge/discharge of battery energy storage in low voltage distribution network with high photovoltaic penetration," *Applied Energy*, vol. 226, pp. 957-966, 2018.

[16] S. Z. Moghaddam, "Generation and transmission expansion planning with high penetration of wind farms considering spatial distribution of wind speed," *International Journal of Electrical Power & Energy Systems*, vol. 106, pp. 232-241, 2019.

[17] T. L. Lee, Y. C. Wang, and J. C. Li *et al*., "Hybrid active filter with variable conductance for harmonic resonance

suppression in industrial power systems," *IEEE Transactions on Industrial Electronics*, vol. 62, no. 2, pp. 746-756, Feb. 2014.

[18] J. Lu, P. Fu, and J. Li *et al*., "A new hybrid filter based on differential current control method for low-order harmonic suppression in Tokamak power system," *International Journal of Energy Research*, vol. 42, no. 1, pp. 82-90, Jan. 2018.

[19] W. Lu, C. Li, and C. Xu, "Sliding mode control of a shunt hybrid active power filter based on the inverse system method," *International Journal of Electrical Power & Energy Systems*, vol. 57, pp. 39-48, 2014.

[20] A. Marzoughi, H. Imaneini, and A. Moeini, "An optimal selective harmonic mitigation technique for high power converters," *International Journal of Electrical Power & Energy Systems*, vol. 49, pp. 34-39, 2013.

[21] Z. Q. Bo, X. N. Lin, and Q. P. Wang *et al*., "Developments of power system protection and control', *Protection and Control of Modern Power Systems*, vol. 1, no.1, pp. 1-8, Jan. 2016.

[22] K. Wang and S. Zhang, "Rainfall-induced landslides assessment in the Fengjie County, Three-Gorge reservoir area, China," *Natural Hazards*, vol. 108, pp. 451-478, 2021.

[23] G. K. Kumaran, P. Rajesh, and S. Kumaravel *et al*., "Two-area power system stability analysis by frequency controller with UPFC synchronization and energy storage systems by optimization approach," *International Review of Applied Sciences and Engineering*, vol. 14, no. 2, pp. 270-284, Feb. 2023.

[24] G. Arunsankar and S. Srinath, "Harmonics mitigation in hybrid shunt active power filter connected renewable energy source using an intelligent controller," *Transactions of the Institute of Measurement and Control*, vol. 43, no. 1, pp. 102-121, Jan. 2021.

[25] C. N. Gnanaprakasam, S. Meena, and M. N. Devi *et al.*, "Robust energy management technique for plug-in hybrid electric vehicle with traffic condition identification," *Applied Soft Computing*, vol. 133, 2023.

[26] V. Vanitha and E. Vallimurugan, "A hybrid approach for optimal energy management system of internet of things enabled residential buildings in smart grid," *International Journal of Energy Research*, vol. 46, no. 9, pp. 12530-12548, Sep. 2022.

[27] A. Micallef, M. Apap, and C. Spiteri-Staines *et al*., "Mitigation of harmonics in grid-connected and islanded microgrids via virtual admittances and impedances," *IEEE Transactions on Smart Grid*, vol. 8, no. 2, pp. 651-661, Feb. 2015.

[28] S. Mikkili and A. K. Panda, "Simulation and real-time implementation of shunt active filter id–iq control strategy for mitigation of harmonics with different fuzzy membership functions," *IET Power Electronics*, vol. 5, no. 9, pp. 1856-1872, Sep. 2012.

[29] R. Manivasagam, A. Al-khaykan, and G. Sudhakaran *et al*., "Hybrid wind-PV farm with STATCOM for damping & control of overall chaotic oscillations in two-area power system using hybrid technique," *Solar Energy*, vol. 262, no. 1, Jan. 2023.

[30] A. K. Panda and S. Mikkili, "FLC based shunt active filter (p–q and Id–Iq) control strategies for mitigation of harmonics with different fuzzy MFs using MATLAB and real-time digital simulator," *International Journal of Electrical Power & Energy Systems*, vol. 47, no. 1, pp. 313-336, Jan. 2013.

[31] J. C. Quiroz, N. Mariun, and M. R. Mehrjou *et al*., "Fault detection of broken rotor bar in LS-PMSM using random forests," *Measurement*, vol. 116, no. 1, pp. 273-280, Jan. 2018.

[32] S. S. Rangarajan, E. R. Collins, and J. C. Fox, "Efficacy of a smart photovoltaic inverter as a virtual detuner for mitigating network harmonic resonance in distribution systems," *Electric Power Systems Research*, vol. 171, no. 1, pp. 175-184, Jan. 2019.

[33] V. Aneesh, "A hybrid technique linked FOPID for a nonlinear system based on closed-loop settling time of plant," *Robotics and Autonomous Systems*, vol. 1, no. 1, Jan. 2024.

[34] P. K. Barik, G. Shankar, and P. K. Sahoo, "Investigations on split-source inverter based shunt active power filter integrated microgrid system for improvement of power quality issues," *Journal of Electrical Engineering & Technology*, vol. 17, no. 4, pp. 2025-2047, Apr. 2022.

[35] M. Büyük, A. Tan, and M. Tümay, "Resonance suppression of LCL filter for shunt active power filter via active damper," *International Journal of Electrical Power & Energy Systems*, vol. 134, no. 1, Jan. 2022.

[36] M. Sivasubramanian, C. S. Boopathi, and S. Vidyasagar *et al*., "Performance evaluation of seven level reduces switch ANPC inverter in shunt active power filter with RBFNN-based harmonic current generation," *IEEE Access*, vol. 10, no. 1, pp. 21497-21508, Jan. 2021.

[37] M. Fallah, J. Modarresi, and H. M. Kojabadi *et al*., "A modified indirect extraction method for a single-phase shunt active power filter with smaller DC-link capacitor size," *Sustainable Energy Technologies and Assessments*, vol. 45, no. 1, Jan. 2021.

[38] M. Iqbal, M. Jawad, and M. H. Jaffery *et al*., "Neural networks based shunt hybrid active power filter for harmonic elimination", *IEEE Access*, vol. 9, no. 1, pp. 69913-69925, Jan. 2021.

[39] P. Abirami and C. N. Ravi, "Enhancing grid stability by maintaining power quality in distribution network using FOPID and ANN controlled shunt active filter," *Environment, Development and Sustainability*, vol. 1, no. 1, pp. 1-28, Jan. 2022.

[40] S. Sharma and V. Verma, "Modified control strategy for shunt active power filter with MRAS-based DC voltage estimation and load current sensor reduction," *IEEE Transactions on Industry Applications*, vol. 57, no. 2, pp. 1652-1663, Feb. 2021.

[41] N. Patel, N. Gupta, and R. C. Bansal, "Combined active power sharing and grid current distortion enhancement-based approach for grid-connected multifunctional photovoltaic inverter," *International Transactions on Electrical Energy Systems*, vol. 30, no. 3, Mar. 2020.

[42] K. Sabanci and S. Balci, "Development of an expression for the output voltage ripple of the DC-DC boost converter circuits by using particle swarm optimization algorithm," *Measurement*, vol. 158, no. 1, pp. 107694, Jan. 2020.

[43] V. Gali, N. Gupta, and R. A. Gupta, "Experimental investigations on multitudinal sliding mode controller-based interleaved shunt APF to mitigate shoot-through and PQ problems under distorted supply voltage conditions," *International Transactions on Electrical Energy Systems*, vol. 29, no. 1, Jan. 2019.

[44] S. R. Das, P. K. Ray, and A. K. Sahoo *et al*., "Improvement of power quality in a three-phase system using an adaline-based multilevel inverter," *Frontiers in Energy Research*, vol. 8, no. 1, Jan. 2020.

[45] A. Gholami, M. Ameri, and M. Zandi *et al*., "A single-diode model for photovoltaic panels in variable environmental conditions: investigating dust impacts with experimental evaluation," *Sustainable Energy Technologies and Assessments*, vol. 47, no. 1, Jan. 2021.

[46] P. Malik, R. Chandel, and S. S. Chandel, "A power prediction model and its validation for a roof top photovoltaic power plant considering module degradation," *Solar Energy*, vol. 224, no. 1, pp. 184-194, Jan. 2021.

[47] Z. Hekss, A. Abouloifa, and I. Lachkar *et al*., "Nonlinear adaptive control design with average performance analysis for photovoltaic system based on half bridge shunt active power filter," *International Journal of Electrical Power & Energy Systems*, vol. 125, no. 1, Jan. 2021.

[48] D. Lu, X. Wang, and F. Blaabjerg, "Impedance-based analysis of DC-link voltage dynamics in voltage-source converters," *IEEE Transactions on Power Electronics*, vol. 34, no. 4, pp. 3973-3985, Apr. 2018.

[49] Z. Hekss, A. Abouloifa, and I. Lachkar *et al.*, "Advanced nonlinear controller of single-phase shunt active power filter interfacing solar photovoltaic source and electrical power grid," *International Transactions on Electrical Energy Systems*, vol. 31, no. 12, Dec. 2021.

[50] S. Echalih, A. Abouloifa, and J. M. Janik *et al*., "Hybrid controller with fuzzy logic technique for three phase half bridge interleaved buck shunt active power filter," *IFAC-Papers Online*, vol. 53, no. 2, pp. 13418-13423, Feb. 2020.

[51] S. Echalih, A. Abouloifa, and I. Lachkar *et al*., "Nonlinear control design and stability analysis of single phase half bridge interleaved buck shunt active power filter," *IEEE Transactions on Circuits and Systems I: Regular Papers*, vol. 69, no. 5, pp. 2117-2128, May 2022.

[52] K. Ishaque, Z. Salam, and G. Lauss, "The performance of perturb and observe and incremental conductance maximum power point tracking method under dynamic weather conditions," *Applied Energy*, vol. 119, no. 1, pp. 228-236, Jan. 2014.

[53] S. Echalih, A. Abouloifa, and I. Lachkar *et al*., "Hybrid automaton-fuzzy control of single phase dual buck half bridge shunt active power filter for shoot through elimination and power quality improvement," *International Journal of Electrical Power & Energy Systems*, vol. 131, no. 1, Jan. 2021.

[54] A. Abouloifa, F. Giri, and I. Lachkar *et al*., "Cascade nonlinear control of shunt active power filters with average performance analysis," *Control Engineering Practice*, vol. 26, no. 1, pp. 211-221, Jan. 2014.

[55] M. Azizi, "Atomic orbital search: a novel metaheuristic algorithm," *Applied Mathematical Modelling*, vol. 93, no. 1, pp. 657-683, Jan. 2021.

[56] Q. Q. Li, Z. C. He, and E. Li, "The feedback artificial tree (FAT) algorithm," *Soft Computing*, vol. 24, no. 1, pp. 13413-13440, Jan. 2020.